Brain Research 1689 (2018) 30–44

Contents lists available at ScienceDirect

Brain Research

journal homepage: www.elsevier.com/locate/bres

Research report

Novel *Drosophila* model for mitochondrial diseases by targeting of a solute carrier protein SLC25A46

Kojiro Suda [a], Ibuki Ueoka [a], Yumiko Azuma [b,c], Yuuka Muraoka [a], Hideki Yoshida [a], Masamitsu Yamaguchi [a,*]

[a] Department of Applied Biology and The Center for Advanced Insect Research, Kyoto Institute of Technology, Matsugasaki, Sakyo-ku, Kyoto 606-8585, Japan
[b] Department of Neurology, Graduate School of Medical Science, Kyoto Prefectural University of Medicine, 465 Kajii-cho, Kamigyo-ku, Kyoto 602-8566, Japan
[c] Department of Molecular Pathobiology of Brain Diseases, Graduate School of Medical Science, Kyoto Prefectural University of Medicine, 465 Kajii-cho, Kamigyo-ku, Kyoto 602-8566, Japan

ARTICLE INFO

Article history:
Received 10 January 2018
Received in revised form 21 March 2018
Accepted 23 March 2018
Available online 28 March 2018

Keywords:
Mitochondrial disease
Solute carrier
Drosophila
Neuron
Neuromuscular junction
ROS

ABSTRACT

Mutations in *SLC25A46* gene have been identified in mitochondrial diseases that are sometimes classified as Charcot-Marie-Tooth disease type 2, optic atrophy and Leigh syndrome. Human SLC25A46 functions as a transporter across the outer mitochondrial membrane. However, it is still unknown how the neurodegeneration occurring in these diseases relates to the loss of SLC25A46 function. *Drosophila* has *CG5755* (*dSLC25A46*) as a single human *SLC25A46* homolog. Here we established pan-neuron specific *dSLC25A46* knockdown flies, and examined their phenotypes. Neuron specific knockdown of *dSLC25A46* resulted in an impaired motility in both larvae and adults. Defects at neuromuscular junctions (NMJs), such as reduced synaptic branch length, decreased number and size of bouton, reduced density and size of active zone were also observed with the *dSLC25A46* knockdown flies. Mitochondrial hyperfusion in synapse at NMJ, accumulation of reactive oxygen species and reduction of ATP were also observed in the *dSLC25A46* knockdown flies. These results indicate that depletion of SLC25A46 induces mitochondrial defects accompanied with aberrant morphology of motoneuron and reduction of active zone that results in defect in locomotive ability. In addition, it is known that *SLC25A46* mutations in human cause optic atrophy and knockdown of *dSLC25A46* induces aberrant morphology of optic stalk of photoreceptor neurons in third instar larvae. Morphology and development of optic stalk of photoreceptor neurons in *Drosophila* are precisely regulated via cell proliferation and migration. Immunocytochemical analyses of subcellular localization of dSLC25A46 revealed that dSLC25A46 localizes not only in mitochondria, but also in plasma membrane. These observations suggest that in addition to the role in mitochondrial function, plasma membrane-localized dSLC25A46 plays a role in cell proliferation and/or migration to control optic stalk formation. The *dSLC25A46* knockdown fly thus recapitulates most of the phenotypes in mitochondrial disease patients, providing a useful tool to study these diseases.

1. Introduction

Solute carriers (SLCs) consists of the largest family of membrane transport proteins in human (Hediger et al., 2004). Phylogenetic analyses have identified 384 unique protein sequences forming 52 distinct SLC families (Rask-Andersen et al., 2013). SLC-transporters localize in the plasma membrane or in intracellular compartment membranes. SLCs regulate the transport of various substrates including inorganic ions, purines, nucleotides, amino acids, sugars, fatty acids, neurotransmitters, and drug molecules across biological membranes (Hediger et al., 2004). Defects in SLCs by mutations or genetic variants, have been suggested as underlying factors in various human diseases such as diabetes, cancer, psychiatric disorders and neurodevelopmental disorders (Rask-Andersen et al., 2013).

Out of fifty-two SLC families, SLC25 family proteins commonly localize in the mitochondria (Hediger et al., 2004). Out of forty-six SLC25 family proteins, only SLC25A46 protein is reported to interact with Mitofusin2. SLC25A46 protein is predicted to have the typical structure of full-size SLC proteins, including two Solcar repeats, each containing two transmembrane domains. SLC25A46 is the most highly expressed in nervous system (Haitina et al., 2006). Other studies predicted SLC25A46 to function as a transporter across the outer mitochondrial membrane (Palmieri, 2013). Dominant or recessive mutations in the *SLC25A46* gene in patients showed cerebellar atrophy, peripheral neuropathy and

Abbreviations: SLC, solute carrier; CNS, central nervous system; NMJ, neuromuscular junction; ROS, reactive oxygen species.

* Corresponding author.
E-mail address: myamaguc@kit.ac.jp (M. Yamaguchi).

https://doi.org/10.1016/j.brainres.2018.03.028
0006-8993/

optic atrophy (Abrams et al., 2015; Charlesworth et al., 2016). This disorder spectrum was defined as hereditary motor sensory neuropathy Type VIB (HMSN6B) that is classified as one of the axonal Charcot-Marie-Tooth (CMT) disease, in Online Mendelian Inheritance in Man (OMIM) (http://www.omim.org/entry/616505). Other studies showed that *SLC25A46* mutations also cause multiple neuropathies including optic atrophy, Leigh syndrome, progressive myoclonic ataxia and lethal congenital pontocerebellar hypoplasia (Charlesworth et al., 2016p. 25; Janer et al., 2016; Nguyen et al., 2017; Wan et al., 2016).

Previous functional study with cultured non-neuron cells revealed the role for SLC25A46 in mitochondrial fission, that is likely mediated by protein networks distinct from the Mitofusin2-Optic atrophy protein1 (MFN2-OPA1) fusion complex (Abrams et al., 2015). More recent studies based on cultured non-neuron cell models suggested that SLC25A46 plays other roles in mitochondrial dynamics by controlling contacts between endoplasmic reticulum (ER) and mitochondria or by regulating MFN1/2 oligomerization (Janer et al., 2016; Steffen et al., 2017). Other studies with *SLC25A46* knockout mice demonstrated predicted phenotypes, including impaired motility, abnormal mitochondria in Purkinje cells and optic atrophy (Li et al., 2017). However, pathological mechanism of diseases caused by SLC25A46 is not fully understood and there is no effective treatment or therapy for CMT disease with mitochondrial defect.

Drosophila has a single homolog for the human *SLC25A46* gene called *CG5755*, which is located on the region 36E4 of the fly 2L chromosome. Because *Drosophila CG5755* and human *SLC25A46* are highly conserved, we designated the *Drosophila CG5755* as *dSLC25A46*. In the present study, we have established a *Drosophila* mitochondrial disease model including CMT targeted to *dSLC25A46*. *Drosophila* has been established as an excellent model for studying various human diseases (Chow and Reiter, 2017). Taking account of the advantages of *Drosophila* as a useful model organism, establishment of *Drosophila* models for mitochondrial disease will contribute to understanding of its pathological mechanism. Our previous studies and other studies revealed that mutants or knockdown of *Drosophila* homolog of the CMT causing genes exhibits deficit in motor abilities of adult flies as well as aberrant morphology of peripheral neurons. These phenotypic characteristics are reminiscent of human CMT patients, suggesting that this is a useful fly model for studying CMT (Bharadwaj et al., 2016; Kyotani et al., 2016; Niehues et al., 2016; Storkebaum et al., 2009). Here, we found that pan-neuron-specific knockdown of *dSLC25A46* results in an impaired motility in both larvae and adults. Defects at neuromuscular junctions (NMJs) were also observed with the *dSLC25A46* knockdown flies. Mitochondrial hyperfusion in synapse at NMJ, accumulation of reactive oxygen species and reduction of ATP were also observed in the knockdown flies. These results indicate that depletion of SLC25A46 induces mitochondrial defects accompanied with aberrant morphology of motoneuron and reduction of active zone that results in defect in locomotive ability. In addition, it is known that *SLC25A46* mutations in human cause optic atrophy and knockdown of *dSLC25A46* induces aberrant morphology of photoreceptor neurons in third instar larvae. These observations suggest that in addition to the role in mitochondrial function, plasma membrane-localized dSLC25A46 plays a role in controlling optic stalk formation.

2. Results

2.1. Comparison of the aa sequence of human SLC25A46, and Drosophila CG5755

A Blast search with human SLC25A46 identified CG5755 in *Drosophila*. The amino acid sequence of *Drosophila* CG5755 was retrieved from UniProt and compared with that of human SLC25 family members using FASTA and BLAST. According to this comparison, high conservation was found between *Drosophila* CG5755 and human SLC25A46, showing 21% identity and 60% similarity. Other SLC25 subfamily proteins in humans were less similar to *Drosophila* CG5755. Human SLC25A46 encodes protein consisting of 418 aa (Fig. 1). The specific protein domains Solcar1 and Solcar2, each containing two transmembrane domains are both highly conserved between CG5755 and SLC25A46, showing 40% identity (75% similarity) and 43% identity (78% similarity), respectively (Fig. 1). In this study, we referred to *Drosophila* CG5755 as *Drosophila* SLC25A46 (dSLC25A46).

2.2. Specificity of the anti-dSLC25A46 antibody and evaluation of knockdown efficiency

We performed qRT-PCR to examine knockdown efficiency. The results showed that mRNA levels of dSLC25A46 reduced to 50.1% and 30.0% in flies carrying *w, UAS-dSLC25A46-IR$_{142-242}$/ w; +; elav-GAL4/+, w; UAS-dSLC25A46-IR$_{207-350}$/+; elav-GAL4/+*, respectively (Fig. 2A), suggesting that *dSLC25A46* is effectively knocked down in these flies. We raised an antibody against a peptide corresponding to amino acid residues 423–436 of dSLC25A46 for immunological studies. In order to confirm the specificity of this antibody, we carried out Western blotting analyses with extracts of larval brain carrying *w; UAS-GFP-IR/+; elav-GAL4/ +, w, UAS-dSLC25A46-IR$_{142-242}$/ w; +; elav-GAL4/+, w; UAS-dSLC25A46-IR$_{207-350}$/+; elav-GAL4/+, w; UAS-dSLC25A46-IR$_{207-350}$; elav-GAL4/+*. In these flies, double-stranded RNA for *GFP* or *dSLC25A46* is specifically expressed in all neurons. Extracts of twenty larval CNS from each strain were prepared and subjected to the Western blotting analyses. Whole procedures were repeated twice. A single band corresponding to an apparent molecular size of 50 kDa was detected (Fig. 2B). The molecular size of this band is similar to that predicted for the aa sequence of dSLC25A46 (50.78 kDa). The intensity of this band was quantified and statistically evaluated. The band was reduced to 52.2% in knockdown flies carrying *w, UAS-dSLC25A46-IR$_{142-242}$/ w; +; elav-GAL4/+* compared to its intensity in control flies carrying *w; UAS-GFP-IR/+; elav-GAL4/+* (Fig. 2C). The intensity was reduced to 46.9% in flies carrying a single copy of *UAS-dSLC25A46-IR$_{207-350}$* (*w; UAS-dSLC25A46-IR$_{207-350}$/+; elav-GAL4/+*) and to 31.4% in those carrying two copies of *UAS-dSLC25A46-IR$_{207-350}$* (*w; UAS-dSLC25A46-IR$_{207-350}$; elav-GAL4/+*) (Fig. 2C). These reductions of the 50 kDa band intensities were statistically significant. These data indicate that the antibody is highly specific to the dSLC25A46 protein and further confirming that dSLC25A46 is effectively knocked down in flies carrying *w, UAS-dSLC25A46-IR$_{142-242}$/w; +; elav-GAL4/+, w; UAS-dSLC25A46-IR$_{207-350}$/+; elav-GAL4/+, w; UAS-dSLC25A46-IR$_{207-350}$; elav-GAL4/+*.

2.3. Subcellular localization of dSLC2546 on larval salivary gland

To further evaluate the specificity of anti-dSLC25A46 antibody, we performed competition experiments with the immunizing peptide (Fig. S1). The dSLC25A46 signals in the cytoplasm, nucleus and plasma membrane were all decreased (Fig. S1C, D) compared to control (Fig. S1A, B). Furthermore, a flip-out experiment was employed to make a somatic clone expressing *dSLC25A46* dsRNA in the salivary glands. In RNAi clones marked with GFP, the intensity of dSLC25A46 signals was extensively reduced (Fig. 3A–D), thus confirming that the anti-dSLC25A46 signals in the cytoplasm, nucleus and plasma membrane truly represent dSLC25A46 protein. Double-immunostaining of larval salivary gland with anti-dSLC25A46 and specific marker antibodies for each of mitochondria, endoplasmic reticulum (ER), Golgi apparatus and plasma membrane were performed. The anti-Discs large (Dlg) antibody

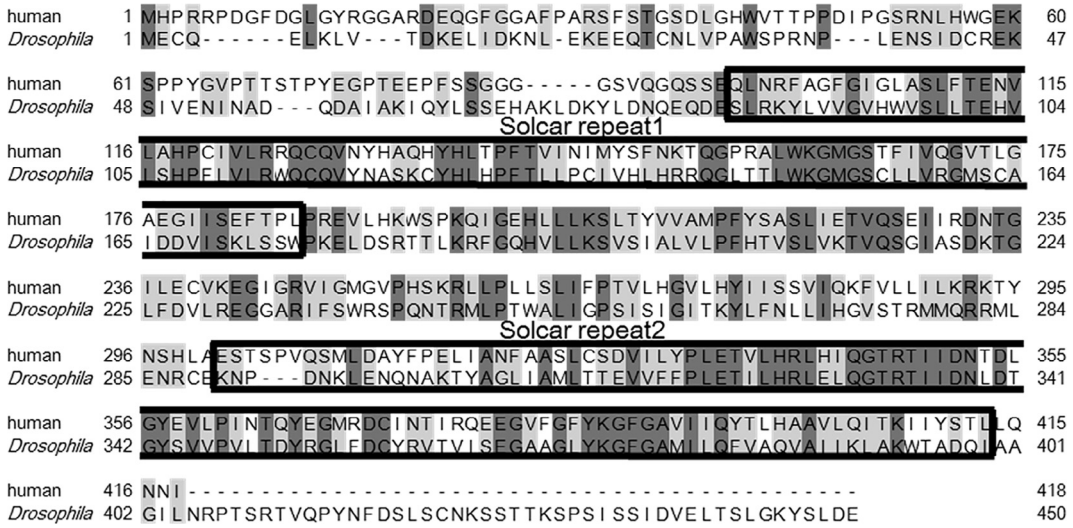

Fig. 1. Sequence Alignment of human SLC25A46 and *Drosophila* SLC25A46. Identical amino acids are dark shaded, and similar or related amino acids are light shaded. Solcar1 and Solcar2 are boxed.

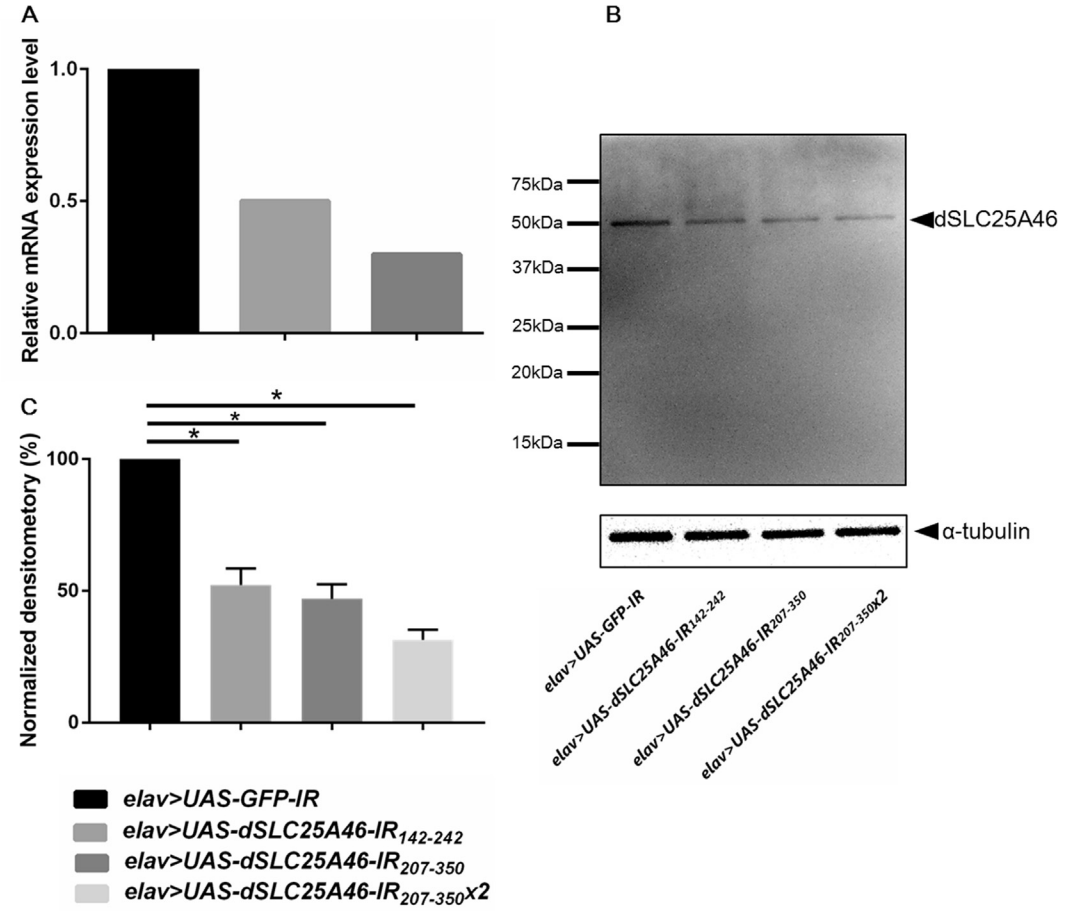

Fig. 2. Knockdown efficiency in larval brains. (A) *dSLC25A46* mRNA levels in larval brains. In *elav> UAS-dSLC25A46-IR* larvae, the mRNA levels of *dSLC25A46* were lower than in control larvae. The mRNA levels were normalized to *GAPDH* mRNA. (B) dSLC25A46 protein levels in larval brains analyzed by Western blotting. Proteins were extracted from larval CNS carrying *elav-GAL4 > UAS-GFP-IR* (*w; UAS-GFP-IR/+; elav-GAL4/+*), *elav-GAL4 > UAS-dSLC25A46-IR$_{142-242}$* (*w, UAS-dSLC25A46-IR$_{142-242}$/w; +; elav-GAL4/+*), *elav-GAL4 > UAS-dSLC25A46-IR$_{207-350}$* (*w; UAS-dSLC25A46-IR$_{207-350}$/+; elav-GAL4/+*), and *elav-GAL4 > UAS-dSLC25A46-IR$_{207-350}$x2* (*w; UAS-dSLC25A46-IR$_{207-350}$; elav-GAL4/+*). The blots were probed with a rabbit anti-dSLC25A46 antibody. The band with an apparent molecular weight of 50 kDa corresponds to dSLC25A46 protein. (C) Quantification of the 50 kDa band with ImageJ. α-tubulin was used as a loading control. $^{*}p < 0.05$, biological replication n = 2.

specifically marks plasma membrane (Huu et al., 2014). The dSLC25A46 signals merge with Dlg signals, indicating localization of dSLC25A46 in plasma membrane (Fig. 3E–H). To test localization of dSLC25A46 in mitochondria, the mitochondria protein HSP60 (Soltys and Gupta, 1996) was labeled with anti-HSP60 antibody. The dSLC25A46 signals clearly merge with HSP60 signals as

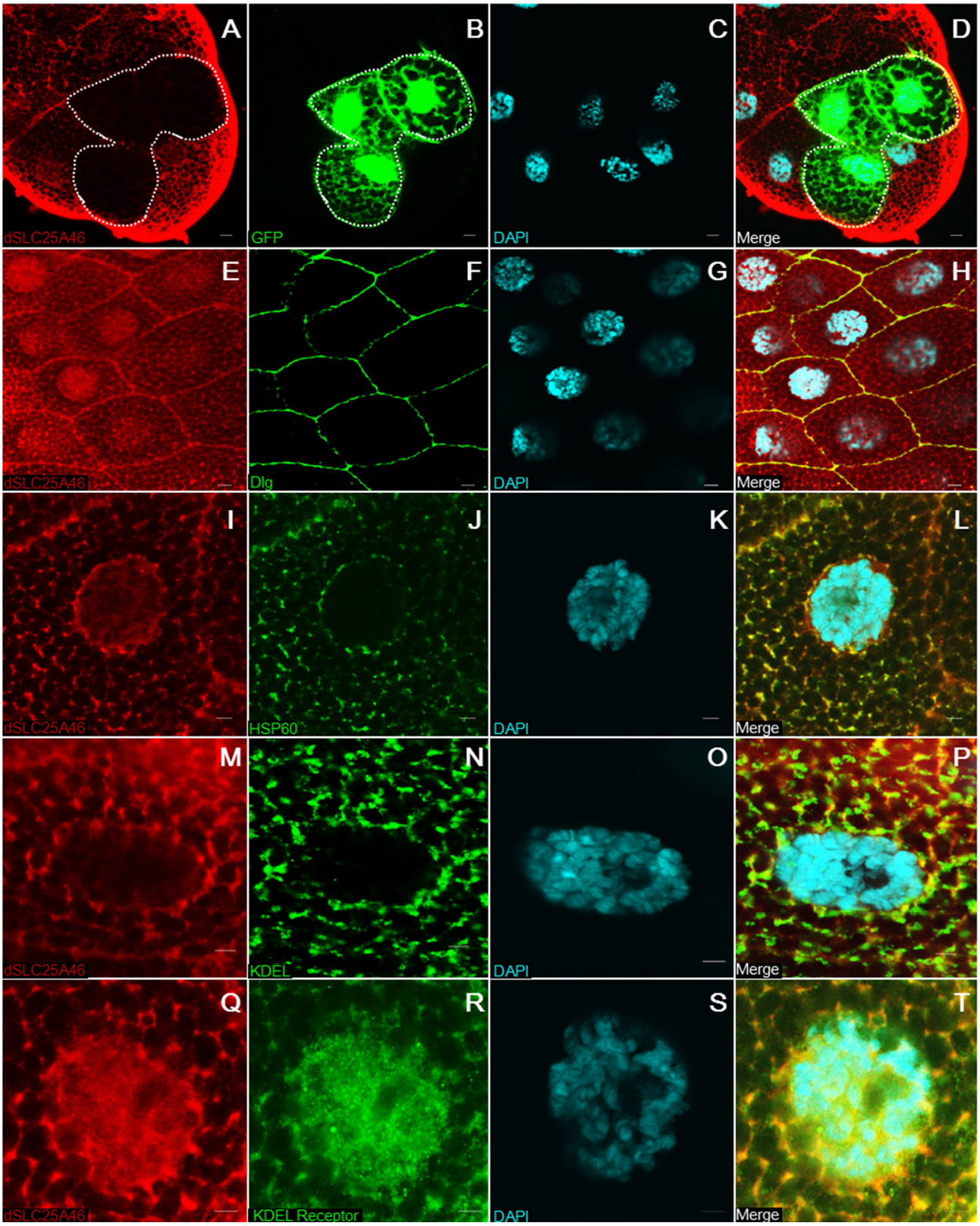

Fig. 3. Immunocytochemistry for dSLC25A46 in the larval salivary gland. Female flies with *hs-flp; Act5C > FRT y FRT > GAL4, UAS-GFP* were crossed with male flies carrying *UAS-dSLC25A46-IR*$_{207-350}$. After flipping-out, third instar larval salivary glands were stained with anti-dSLC25A46 antibody (A). GFP clone (B) and DAPI signals (C) are also shown. Third instar larval salivary glands from Canton S (E-T) were stained with anti-dSLC25A46 antibody (E, I, M, Q), anti-Dlg IgG (F), anti-HSP60 IgG (J), anti-KDEL IgG (N), anti-KDEL receptor IgG (R), and DAPI (G, K, O, S). Merged confocal images are shown in (D, H, L, P, T). Bars indicate 20 μm (A–D), 10 μm (E–H) and 5 μm (I–P).

expected (Fig. 3I–L). The anti-KDEL antibody has been commonly used as the ER marker (Charroux and Royet, 2013) which labels the sequence Lys-Asp-Glu-Leu (KDEL), or a closely related sequence, that is present at the carboxyl terminus of ER soluble and some membrane proteins (Munro and Pelham, 1987; Pelham, 1990, 1988; Teasdale and Jackson, 1996). The dSLC25A46

signals at least partially merge with KDEL signals, suggesting some fraction of dSLC25A46 localize on ER (Fig. 3 M–P). The anti-KDEL receptor antibody has been used as marker of Golgi apparatus (Huu et al., 2014). KDEL receptor is an integral membrane protein which mediates the retrieval of solute resident proteins from Golgi apparatus to the ER (Lewis and Pelham, 1992, 1990; Tang et al., 1993; Teasdale and Jackson, 1996). The dSLC25A46 signals merge with KDEL receptor signals (Fig. 3Q–T). These results revealed that dSLC25A46 localizes not only in mitochondria, but also in plasma membrane and other subcellular organelles such as ER and Golgi apparatus.

2.4. Knockdown of dSLC25A46 causes locomotor defects in both larval and adult stages

Flies carrying *UAS-dSLC25A46-IR* were crossed with the *elav-GAL4* driver strain to specifically knockdown *dSLC25A46* in *Drosophila* pan-neurons. To examine the effect of *dSLC25A46* knockdown on locomotor abilities, a crawling assay for the larval stage and a climbing assay for the adult stage were performed. In the larval stage, *dSLC25A46* knockdown larvae exhibited decreases in motion speed. The average speed of knockdown larvae reduced by 0.4 mm/s in knockdown flies carrying *w, UAS-dSLC25A46-IR$_{142-242}$/w; +; elav-GAL4/+* compared with its speed in control flies carrying *w/+; +; elav-GAL4/+* (Fig. 4A). The average speed was reduced to 0.7 mm/s in flies carrying a single copy of *UAS-dSLC25A46-IR$_{207-350}$* (*w; UAS-dSLC25A46-IR$_{207-350}$/+; elav-GAL4/+*) and to 0.8 mm/s in those carrying two copies of *UAS-dSLC25A46-IR$_{207-350}$* (*w; UAS-dSLC25A46-IR$_{207-350}$; elav-GAL4/+*) (Fig. 4A). These reductions were statistically significant. The defect in locomotor abilities of neuron-specific *dSLC25A46* knockdown flies was also observed at the adult stage (Fig. 4B). The knockdown flies (*w, UAS-dSLC25A46-IR$_{142-242}$/w; +; elav-GAL4/+* and *w; UAS-dSLC25A46-IR$_{207-350}$/+; elav-GAL4/+*) started to exhibit a decrease in mobility at day 3 after eclosion. At 28 days old, the climbing ability of these flies reduced considerably to 30% and continued to decrease compared with that of control flies carrying *w; UAS-GFP-IR/+; elav-GAL4/+* (Fig. 4B). These results indicated that *dSLC25A46* has an important function in regulating locomotion.

2.5. dSLC25A46 plays an important role in synapse structure formation at neuromuscular junctions in third instar larvae

The above-mentioned results on locomotor defects suggested that *dSLC25A46* might have a function in motor neurons. Therefore, we analyzed the morphology of motor neuron presynaptic and postsynaptic terminals at NMJs in *dSLC25A46* knockdown larvae (Fig. 5A). *Drosophila* larval NMJ is a well-established system for studying synaptic functions and morphology (Keshishian et al., 1996). Termini of larval segmental nerves form a series of varicosities where they contact and innervate muscles. These "boutons" contain active zones where neurotransmitters are released and have a stereotyped beads-on-a-string pattern.

The NMJ branch length was reduced to 36.5% in knockdown flies carrying *w, UAS-dSLC25A46-IR$_{142-242}$/w; +; elav-GAL4/+* compared with its length in control flies carrying *w; UAS-GFP-IR/+; elav-GAL4/+* (Fig. 5B). The length was reduced to 75.3% in flies carrying a single copy of *UAS-dSLC25A46-IR$_{207-350}$* (*w; UAS-dSLC25A46-IR$_{207-350}$/+; elav-GAL4/+*) and to 62.2% in those carrying two copies of *UAS-dSLC25A46-IR$_{207-350}$* (*w; UAS-dSLC25A46-IR$_{207-350}$; elav-GAL4/+*) (Fig. 5B). These reductions were statistically significant.

The number of 1b boutons was reduced to 52.0% in knockdown flies carrying *w, UAS-dSLC25A46-IR$_{142-242}$/w; +; elav-GAL4/+* compared with its length in control flies carrying *w; UAS-GFP-IR/+; elav-GAL4/+* (Fig. 5C). The bouton size was reduced to 60.4% in flies carrying a single copy of *UAS-dSLC25A46-IR$_{207-350}$* (*w; UAS-dSLC25A46-IR$_{207-350}$/+; elav-GAL4/+*) and to 73.2% in those carrying two copies of *UAS-dSLC25A46-IR$_{207-350}$* (*w; UAS-dSLC25A46-IR$_{207-350}$; elav-GAL4/+*) (Fig. 5C). These reductions were statistically significant.

The size of 1b boutons was reduced to 46.2% in knockdown flies carrying *w, UAS-dSLC25A46-IR$_{142-242}$/w; +; elav-GAL4/+* compared with its length in control flies carrying *w; UAS-GFP-IR/+; elav-GAL4/+* (Fig. 5D). The bouton size was reduced to 96.5% in flies carrying a single copy of *UAS-dSLC25A46-IR$_{207-350}$* (*w; UAS-dSLC25A46-IR$_{207-350}$/+; elav-GAL4/+*) and to 42.4% in those carrying two copies of *UAS-dSLC25A46-IR$_{207-350}$* (*w; UAS-dSLC25A46-IR$_{207-350}$; elav-GAL4/+*) (Fig. 5D). Except for the data with flies carrying a single

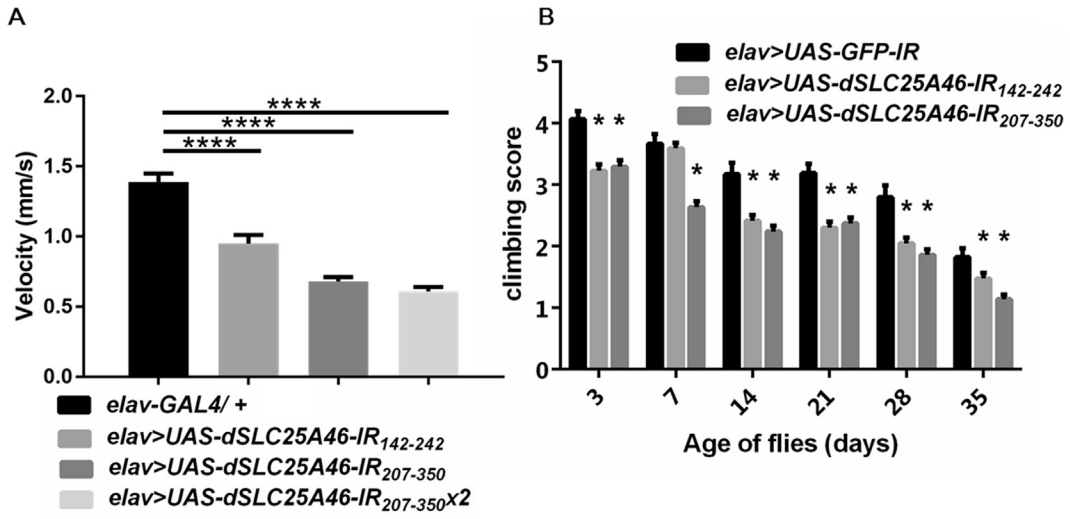

Fig. 4. Locomotor dysfunction in *dSLC25A46* knockdown flies. (A) Crawling assay. Knockdown of *dSLC25A46* in pan-neurons exerted negative effects on the crawling ability of larvae. Quantified data of average crawling speed of flies carrying *elav-GAL4/+* (*w/+; +; elav-GAL4/+*, n = 104), *elav-GAL4 > UAS-dSLC25A46-IR$_{142-242}$* (*w, UAS-dSLC25A46-IR$_{142-242}$/w; +; elav-GAL4/+*, n = 104), *elav-GAL4 > UAS-dSLC25A46-IR$_{207-350}$* (*w; UAS-dSLC25A46-IR$_{207-350}$/+; elav-GAL4/+*, n = 103), and *elav-GAL4 > UAS-dSLC25A46-IR$_{207-350}$x2* (*w; UAS-dSLC25A46-IR$_{207-350}$; elav-GAL4/+*, n = 76). The knockdown larvae crawled more slowly than the control larvae. $^{****}p < 0.001$. (B) Climbing assay. Knockdown of *dSLC25A46* in pan-neurons causes a decrease in climbing ability in adults. $^{*}p < 0.05$. Technical replication n = 5. *elav-GAL4 > UAS-GFP-IR* (*w; UAS-GFP-IR/+; elav-GAL4/+*, n = 100), *elav-GAL4 > UAS-dSLC25A46-IR$_{142-242}$* (*w, UAS-dSLC25A46-IR$_{142-242}$/w; +; elav-GAL4/+*, n = 251), and *elav-GAL4 > UAS-dSLC25A46-IR$_{207-350}$* (*w; UAS-dSLC25A46-IR$_{207-350}$/+; elav-GAL4/+*, n = 240).

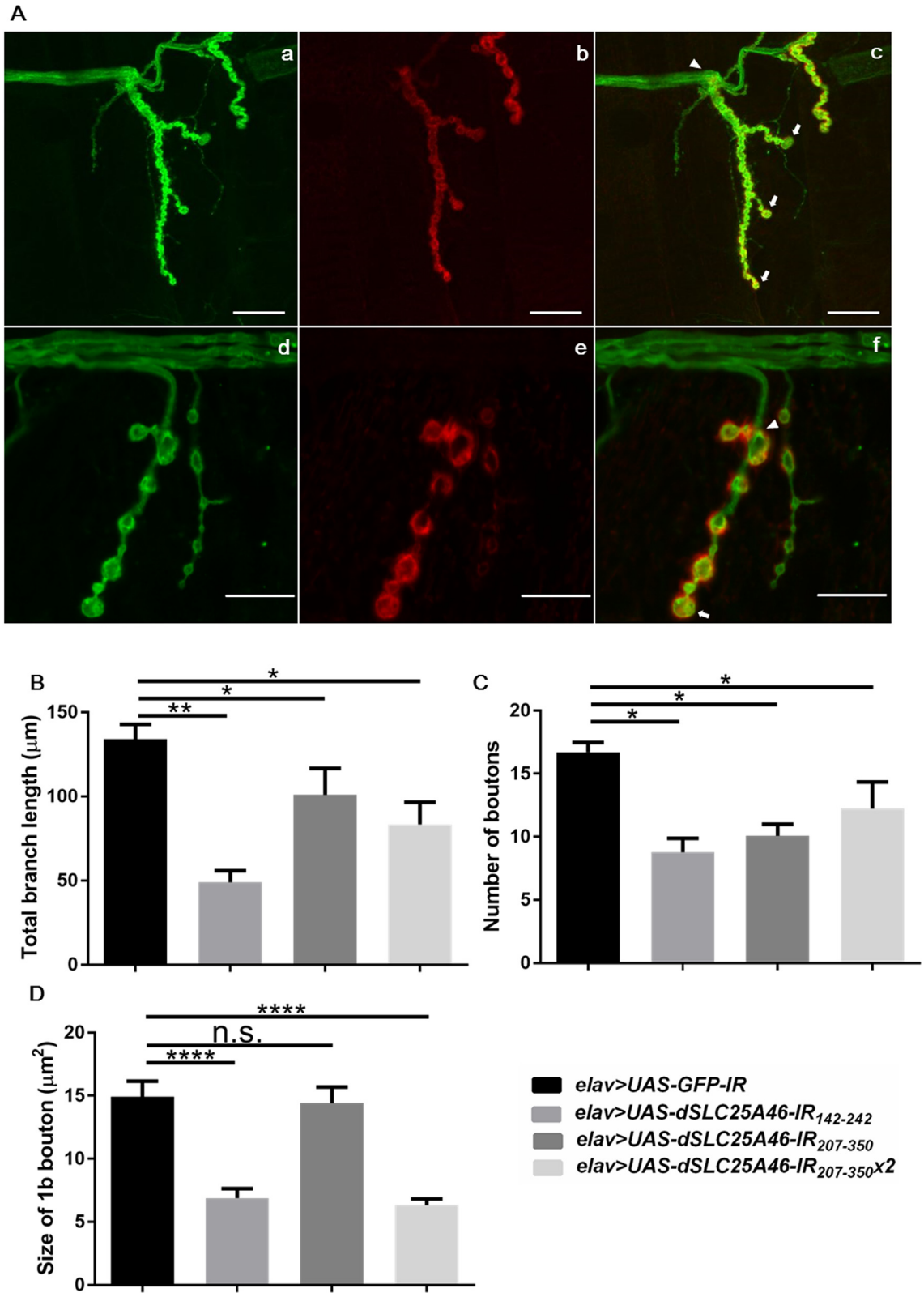

Fig. 5. Knockdown of *dSLC25A46* causes abnormal morphology of synapse at NMJs in muscle 4 of third instar larvae. (A) Images show NMJs that were double-stained with anti-HRP (green) and anti-Dlg (red). NMJs of flies carrying *elav-GAL4 > UAS-GFP-IR* (*w; UAS-GFP-IR/+; elav-GAL4/+*) (a–c), *elav-GAL4 > UAS-dSLC25A46-IR$_{207-350}$x2* (*w; UAS-dSLC25A46-IR$_{207-350}$; elav-GAL4/+*) (d–f) are shown. Length of synaptic branches are measured from white arrowhead to white arrow. Scale bars indicate 10 μm (a–f). (B–D) The quantified data. In *dSLC25A46* knockdown larvae, length of synaptic branches is reduced (B), number and size of bouton are decreased, (C, D) compared with the control larvae ($^{*}p < 0.05$ and $^{**}p < 0.01$, $^{****}p < 0.001$). *elav-GAL4 > UAS-GFP-IR* (*w; UAS-GFP-IR/+; elav-GAL4/+*, n = 10), *elav-GAL4 > UAS-dSLC25A46-IR$_{142-242}$* (*w, UAS-dSLC25A46-IR$_{142-242}$/w; +; elav-GAL4/+*, n = 13), *elav-GAL4 > UAS-dSLC25A46-IR$_{207-350}$* (*w; UAS-dSLC25A46-IR$_{207-350}$/+; elav-GAL4/+*, n = 13), and *elav-GAL4 > UAS-dSLC25A46-IR$_{207-350}$x2* (*w; UAS-dSLC25A46-IR$_{207-350}$; elav-GAL4/+*, n = 9).

copy of *UAS-dSLC25A46-IR$_{207-350}$*, these reduction were statistically significant.

These results indicate that *dSLC25A46* plays an important role in regulating synapse structure formation at NMJs, and locomotor dysfunction might be caused by aberrant morphology of motor neuron presynaptic and postsynaptic terminals in third instar larvae.

2.6. dSLC25A46 plays an important role in active zone structure formation at neuromuscular junctions in third instar larvae

In presynaptic membrane, synaptic vesicles fuse at a specialized membrane domain called the active zone. Neurotransmitters are released at active zones. Therefore, we analyzed the morphology of active zone at NMJs in *dSLC25A46* knockdown larvae (Fig. 6A). The Bruchpilot (Brp), which is a central compartment of electron-dense cytomatrix at active zone, serves as a marker for active zone. In flies carrying two copies of *UAS-dSLC25A46-IR$_{207-350}$* (*w; UAS-dSLC25A46-IR$_{207-350}$; elav-GAL4/+*), the density and size of active zones reduced to 72.0%, 73.6% respectively compared with control larvae carrying *w; UAS-GFP-IR/+; elav-GAL4/+* (Fig. 6B, C). These reductions were statistically significant. The density and size of active zones of other knockdown flies appeared to be decreased, although the difference was not statistically significant. The reduction with single copy knockdown flies was not statistically significant, probably due to the less efficient knockdown of *dSLC25A46* (Fig. 6B, C). The number of active zones is not different between *dSLC25A46* knockdown and control flies (Fig. 6D). These results suggest that *dSLC25A46* plays an important role in regulating active zone structure formation at NMJs, and neuronal dysfunction might be caused by decreased synaptic vesicles containing neurotransmitters.

2.7. dSLC25A46 plays an important role in regulating dynamics of mitochondria at neuromuscular junctions in third instar larvae

SLC25A46 has function in mitochondrial fission in cultured cells (Abrams et al., 2015). Therefore, we analyzed the morphology of mitochondria at NMJs in *dSLC25A46* knockdown larvae (Fig. 7A). Mitochondria in NMJ are detected by overexpressed GFP targeted to mitochondria (Pilling et al., 2006). In flies carrying *UAS-dSLC25A46-IR$_{142-242}$* or *UAS-dSLC25A46-IR$_{207-350}$* (*w, UAS-dSLC25A46-IR$_{142-242}$/w; +; D42-GAL4, UAS-mitoGFP/+* or *w/UAS-dSLC25A46-IR$_{207-350}$/+; D42-GAL4, UAS-mitoGFP/+*), the density of mitochondria increased to 141.4%, 153.1% respectively and the size of mitochondria also increased to 139.5%, 155.4% respectively compared with control larvae carrying *w; UAS-beta gal-IR/+; D42-GAL4, UAS-mitoGFP/+* (Fig. 7B, C). The number of mitochondria is not different between *dSLC25A46* knockdown and control flies (Fig. 7D). These results suggest that hyperfused mitochondria accumulate in NMJ by the lack of mitochondrial dynamics or mitochondria are morphologically elongated under the lack of dSLC25A46 conditions. Accumulation of the defective mitochondria at NMJs might cause neuronal dysfunction and aberrant morphology of motor neuron presynaptic and postsynaptic terminals in third instar larvae.

2.8. dSLC25A46 knockdown increases reactive oxygen species in central nerves system of third instar larvae

The above-mentioned results on mitochondrial aberrant morphology suggested that *dSLC25A46* might have a role in mitochondrial function. Therefore, we analyzed the ROS level as oxidative stress marker of mitochondria in larval central nervous system (CNS) (Fig. 8A). The intensity of ROS signal was increased to 170.6% in knockdown flies carrying *w, UAS-dSLC25A46-IR$_{142-242}$/w; +; elav-GAL4/+* compared with its intensity in control flies carrying *w; UAS-GFP-IR/+; elav-GAL4/+* (Fig. 8B). The intensity was increased to 134.0% in flies carrying a single copy of *UAS-dSLC25A46-IR$_{207-350}$* (*w; UAS-dSLC25A46-IR$_{207-350}$/+; elav-GAL4/+*) and to 282.9% in those carrying two copies of *UAS-dSLC25A46-IR$_{207-350}$* (*w; UAS-dSLC25A46-IR$_{207-350}$; elav-GAL4/+*) (Fig. 8B). Except for the data with flies carrying a single copy of *UAS-dSLC25A46-IR$_{142-242}$*, these increases were statistically significant. These results suggest that mitochondrial function is defective in *dSLC25A46* knockdown flies.

2.9. dSLC25A46 knockdown decreases level of ATP at in larval central nerves system

To further confirm the mitochondrial defect in *dSLC25A46* knockdown flies, we analyzed the ATP level as an indicator of mitochondrial dysfunction. The ATP level was decreased to 43.2% in knockdown larvae carrying *w, UAS-dSLC25A46-IR$_{142-242}$/w; +; elav-GAL4/+* compared with its level in control flies carrying *w; UAS-GFP-IR/+; elav-GAL4/+* (Fig. 9). The ATP level was decreased to 48.0% in flies carrying a single copy of *UAS-dSLC25A46-IR$_{207-350}$* (*w; UAS-dSLC25A46-IR$_{207-350}$/+; elav-GAL4/+*). In flies carrying two copies of *UAS-dSLC25A46-IR$_{207-350}$* (*w; UAS-dSLC25A46-IR$_{207-350}$; elav-GAL4/+*), the level of ATP reduced to 35.0% compared to control larvae carrying *w; UAS-GFP-IR/+; elav-GAL4/+* (Fig. 9). These results taken together with those on ROS production indicate that mitochondrial function is defective in *dSLC25A46* knockdown larvae. Accumulation of the defective mitochondria at NMJs very likely cause neuronal dysfunction and aberrant morphology of motor neuron.

2.10. Knockdown of dSLC25A46 induces axonal targeting aberrations and abnormal morphology of photoreceptor neuron

It is known that *SLC25A46* mutations in human cause optic atrophy. Therefore, we analyzed the morphology of photoreceptor neuron in *dSLC25A46* knockdown larvae. In *Drosophila* eye, it is well known that the projection of axons from photoreceptor cell neurons innervate the centers of the brain to produce visual connections. The differentiating photoreceptor cell neurons of the developing *Drosophila* eye form an axonal bundle, that targets into the different layers of the brains. Each ommatidium of the *Drosophila* eye is composed of eight photoreceptors (R1–R8). R1–R6 neurons innervates lamina and R7–R8 neurons further extends into medulla of the brain. The Chaoptin is widely used as a marker for retinal axons and their projections to the brain. In the control eye imaginal disc, photoreceptor cell neurons visualized by anti-Chaoptin antibody innervate both medulla and lamina in the brain and forms a characteristic "inverted cap" like orientation (Fig. 10A). In flies carrying *w, UAS-dSLC25A46-IR$_{142-242}$/w; +; elav-GAL4/+, w; UAS-dSLC25A46-IR$_{207-350}$/+; elav-GAL4/+, w; UAS-dSLC25A46-IR$_{207-350}$; elav-GAL4/+*, R1-R6 photoreceptor cell neurons project to lamina normally, while aberrations in projection of R7-R8 into medulla were observed in 43%, 31% and 33% of eye discs, respectively (Fig. 10B). In addition, the quantification of optic stalk length and diameter clearly showed that the ratio of diameter per length of knockdown larvae (*w; UAS-dSLC25A46-IR$_{207-350}$; elav-GAL4/+*) was increased to 247% compared to that of control larvae (Fig. 10C). This increase was statistically significant. The ratio of single copy knockdown flies was not significantly increased, probably due to the less efficient knockdown of *dSLC25A46* (Fig. 10C). These results suggest that *dSLC25A46* plays a role in axonal targeting and morphology of photoreceptor neuron.

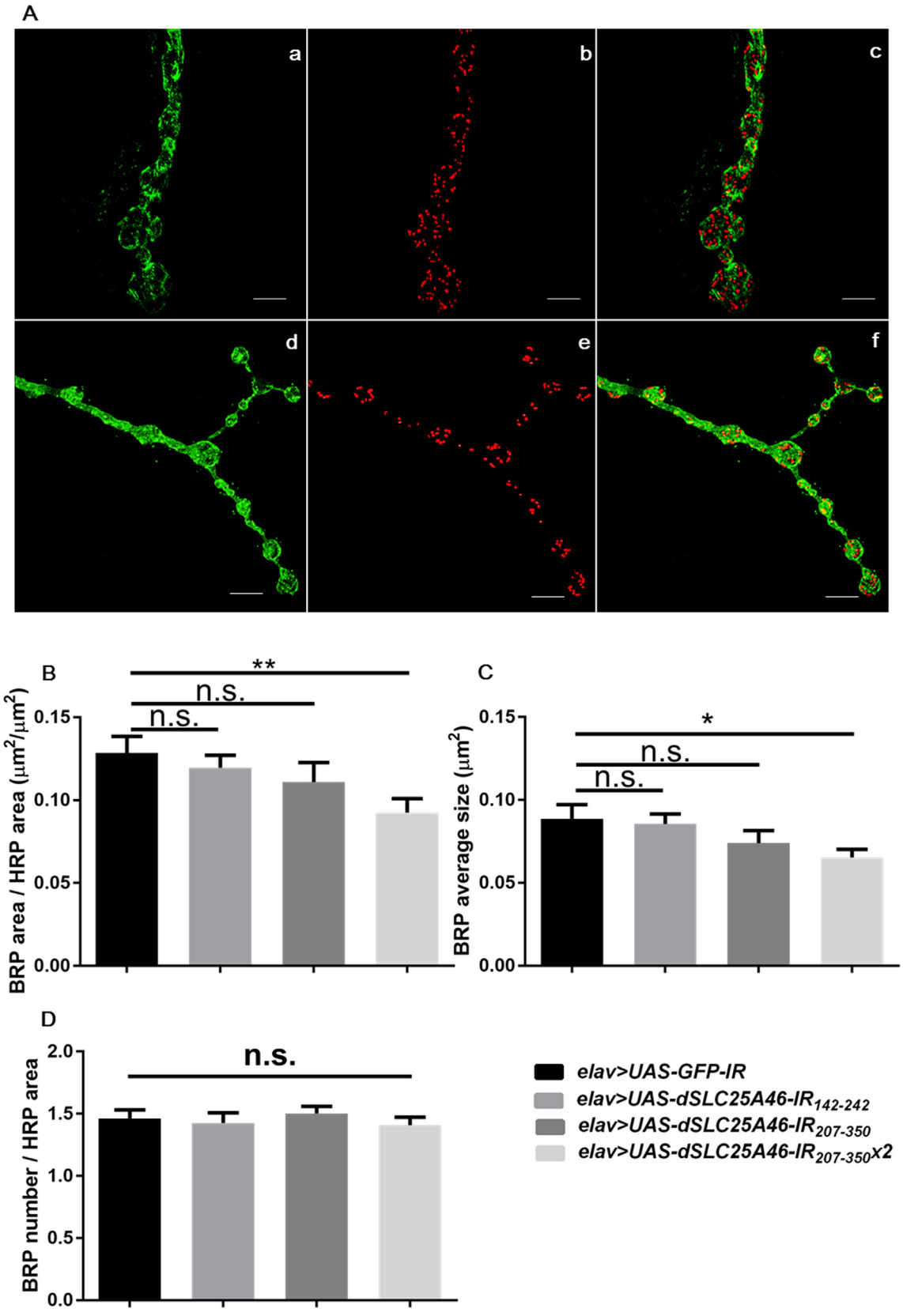

Fig. 6. Knockdown of *dSLC25A46* induces reduced active zone at NMJs in muscle 4 of third instar larvae. (A) Images show NMJs that were double-stained with anti-HRP (green) and anti-Brp (red). NMJs of flies carrying *elav-GAL4 > UAS-GFP-IR* (*w; UAS-GFP-IR/+; elav-GAL4/+*) (a–c), *elav-GAL4 > UAS-dSLC25A46-IR$_{207-350}$x2* (*w; UAS-dSLC25A46-IR$_{207-350}$; elav-GAL4/+*) (d–f) are shown. Scale bars indicate 5 μm (a–f). (B–D) The quantified data. In *dSLC25A46* knockdown larvae, the density and size of active zones are reduced (B, C) compared with the control larvae ($^{*}p < 0.05$ and $^{**}p < 0.01$). The number of active zones is not different between *dSLC25A46* knockdown and control flies (D). *elav-GAL4 > UAS-GFP-IR* (*w; UAS-GFP-IR/+; elav-GAL4/+*, n = 6), *elav-GAL4 > UAS-dSLC25A46-IR$_{142-242}$* (*w, UAS-dSLC25A46-IR$_{142-242}$/w; +; elav-GAL4/+*, n = 9), *elav-GAL4 > UAS-dSLC25A46-IR$_{207-350}$* (*w; UAS-dSLC25A46-IR$_{207-350}$/+; elav-GAL4/+*, n = 8), and *elav-GAL4 > UAS-dSLC25A46-IR$_{207-350}$x2* (*w; UAS-dSLC25A46-IR$_{207-350}$; elav-GAL4/+*, n = 8).

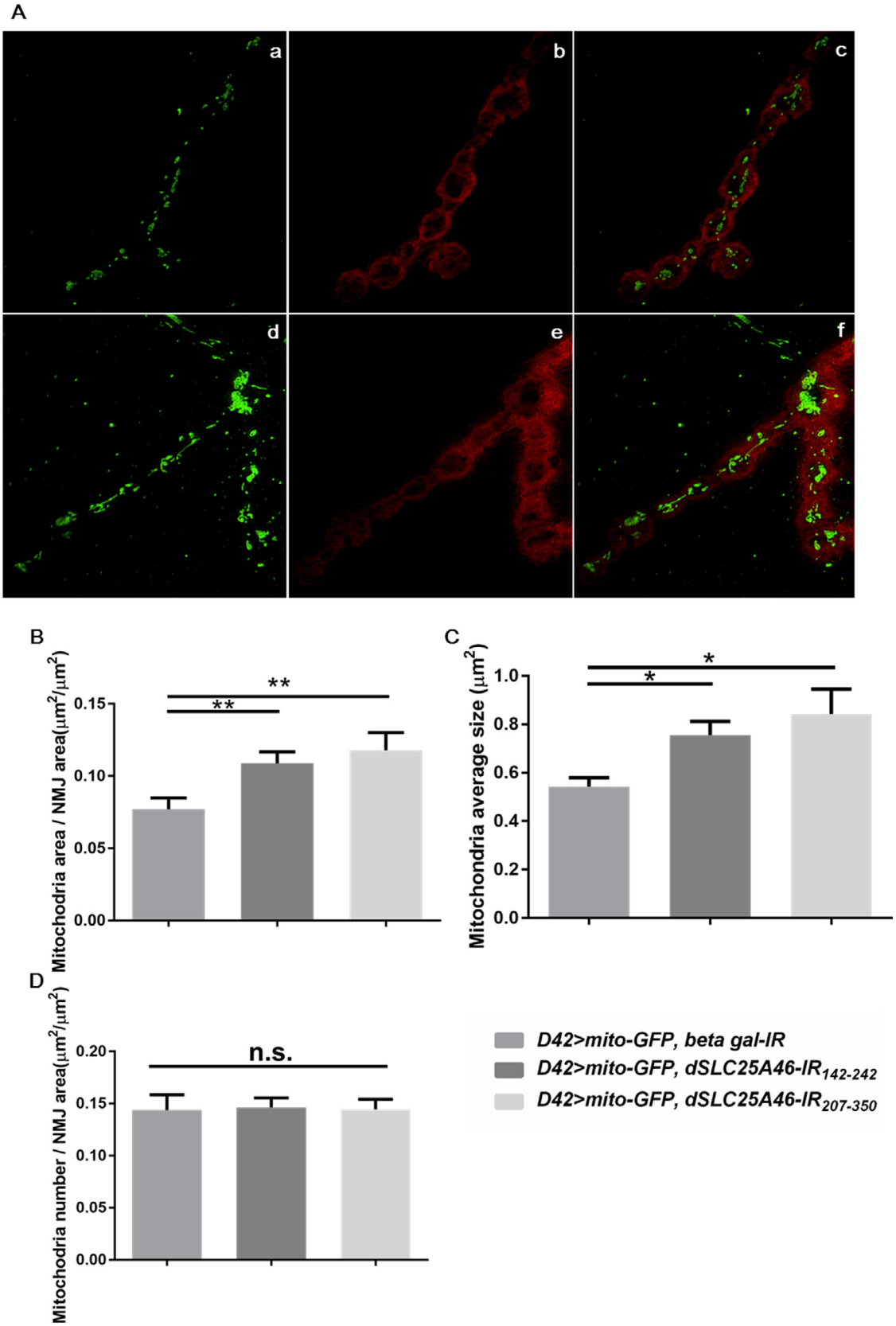

Fig. 7. Knockdown of *dSLC25A46* causes abnormal mitochondrial dynamics at NMJs in muscle 4 of third instar larvae. (A) Images show NMJs that were double-stained with mito-GFP (green) and anti-Dlg (red). NMJs of flies carrying *D42-GAL4 > UAS-beta gal-IR, UAS-mitoGFP* (*w; UAS-beta gal-IR/+; D42-GAL4, UAS-mitoGFP/+*) (a–c), *D42-GAL4 > UAS-dSLC25A46-IR$_{142–242}$, UAS-mitoGFP* (*w, UAS-dSLC25A46-IR$_{142–242}$/w; +; D42-GAL4, UAS-mitoGFP/+*) (d–f) are shown. Scale bars indicate 5 μm (a–f). (B–D) The quantified data. In *dSLC25A46* knockdown larvae, the density and size of mitochondria are increased (B, C) compared with the control larvae ($^{*}p < 0.05$ and $^{**}p < 0.01$). The number of active zones is not different between *dSLC25A46* knockdown and control flies (D). *D42-GAL4 > UAS-beta gal-IR, UAS-mitoGFP* (*w; UAS-beta gal-IR/+; D42-GAL4, UAS-mitoGFP/+*, n = 5), *D42-GAL4 > UAS-dSLC25A46-IR$_{142–242}$, UAS-mitoGFP* (*w, UAS-dSLC25A46-IR$_{142–242}$/w; +; D42-GAL4, UAS-mitoGFP/+*, n = 13), *D42-GAL4 > UAS-dSLC25A46-IR$_{207–350}$, UAS-mitoGFP* (*w/ UAS-dSLC25A46-IR$_{207–350}$/+; D42-GAL4, UAS-mitoGFP/+*, n = 10).

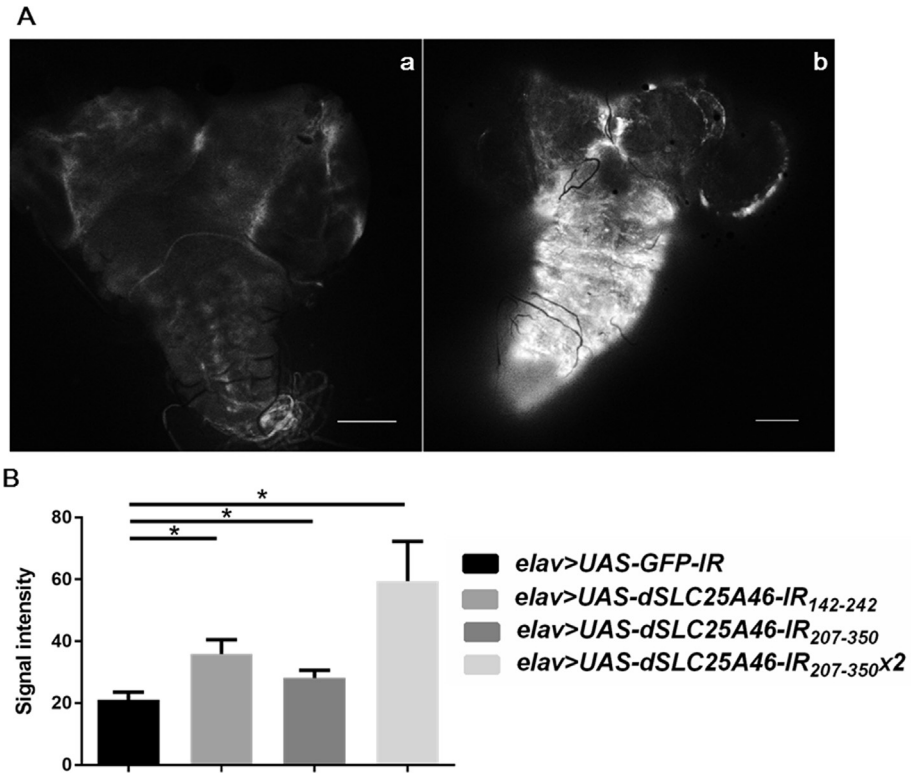

Fig. 8. *dSLC25A46* knockdown increases reactive oxygen species in central nerves system of third instar larvae. (A) Third instar larval CNS were stained with CM-H2DCFDA. Images of *elav-GAL4 > UAS-GFP-IR* (*w; UAS-GFP-IR/+; elav-GAL4/+*) (a) and *elav-GAL4 > UAS-dSLC25A46-IR$_{207-350}$x2* (*w; UAS-dSLC25A46-IR$_{207-350}$; elav-GAL4/+*) (b) are shown. Scale bars indicate 100 μm (B) The quantified data. In *dSLC25A46* knockdown larvae, ROS signals are increased. $^{*}p < 0.05$. *elav-GAL4 > UAS-GFP-IR* (*w; UAS-GFP-IR/+; elav-GAL4/+*, n = 4), *elav-GAL4 > UAS-dSLC25A46-IR$_{142-242}$* (*w, UAS-dSLC25A46-IR$_{142-242}$/w; +; elav-GAL4/+*, n = 4), *elav-GAL4 > UAS-dSLC25A46-IR$_{207-350}$* (*w; UAS-dSLC25A46-IR$_{207-350}$/+; elav-GAL4/+*, n = 4), and *elav-GAL4 > UAS-dSLC25A46-IR$_{207-350}$x2* (*w; UAS-dSLC25A46-IR$_{207-350}$; elav-GAL4/+*, n = 8).

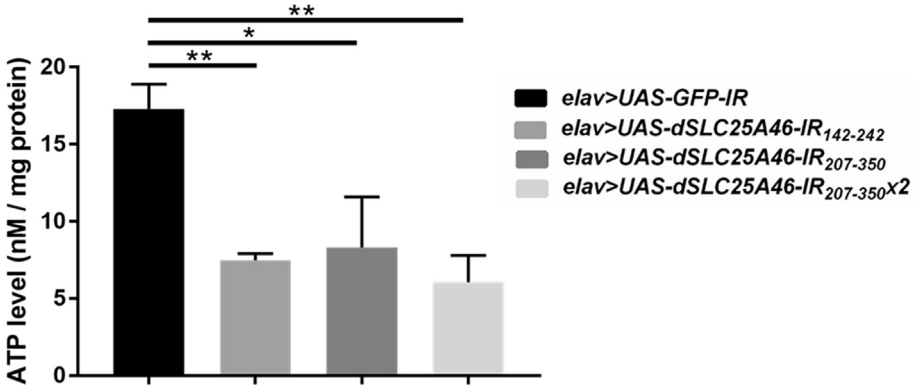

Fig. 9. *dSLC25A46* knockdown decreases level of ATP at in larval central nerves system. In *dSLC25A46* knockdown larvae, ATP level are decreased. $^{*}p < 0.05$. n = 3. *elav-GAL4 > UAS-GFP-IR* (*w; UAS-GFP-IR/+; elav-GAL4/+*), *elav-GAL4 > UAS-dSLC25A46-IR$_{142-242}$* (*w, UAS-dSLC25A46-IR$_{142-242}$/w; +; elav-GAL4/+*), *elav-GAL4 > UAS-dSLC25A46-IR$_{207-350}$* (*w; UAS-dSLC25A46-IR$_{207-350}$/+; elav-GAL4/+*), and *elav-GAL4 > UAS-dSLC25A46-IR$_{207-350}$x2* (*w; UAS-dSLC25A46-IR$_{207-350}$; elav-GAL4/+*).

2.11. Knockdown of dSLC25A46 does not affect in the lifespan of adult flies

We analyzed the effect of neuron-specific *dSLC25A46* knockdown on the survival of flies. The numbers of knockdown flies carrying *w, UAS-dSLC25A46-IR$_{142-242}$/w; +; elav-GAL4/+, w; UAS-dSLC25A46-IR$_{207-350}$/+; elav-GAL4/+* and control flies carrying *w; UAS-GFP-IR/+; elav-GAL4/+* that were still alive were recorded every three days until the last flies died (Fig. 11). There is no significant difference in the median lifespan of control and *dSLC25A46* knockdown flies (Log-rank test, n = 100). Therefore, *dSLC25A46* knockdown does not affect in the lifespan of adult flies.

3. Discussion

In order to clarify whether or not disruption of the physiological functions of *dSLC25A46* are important for the development of neurodegeneration, we have here established fly models in which the *dSLC25A46* gene is knocked down. We revealed that neuron-specific knockdown of *dSLC25A46* induced locomotor defects in both larval and adult stages, defects in motoneurons and mitochondria at NMJs and aberrant morphology of photoreceptor neurons, that are accompanied with accumulation of ROS and reduction of ATP. These observations indicate that decreased level of *dSLC25A46* induces the mitochondrial dysfunction as a primary

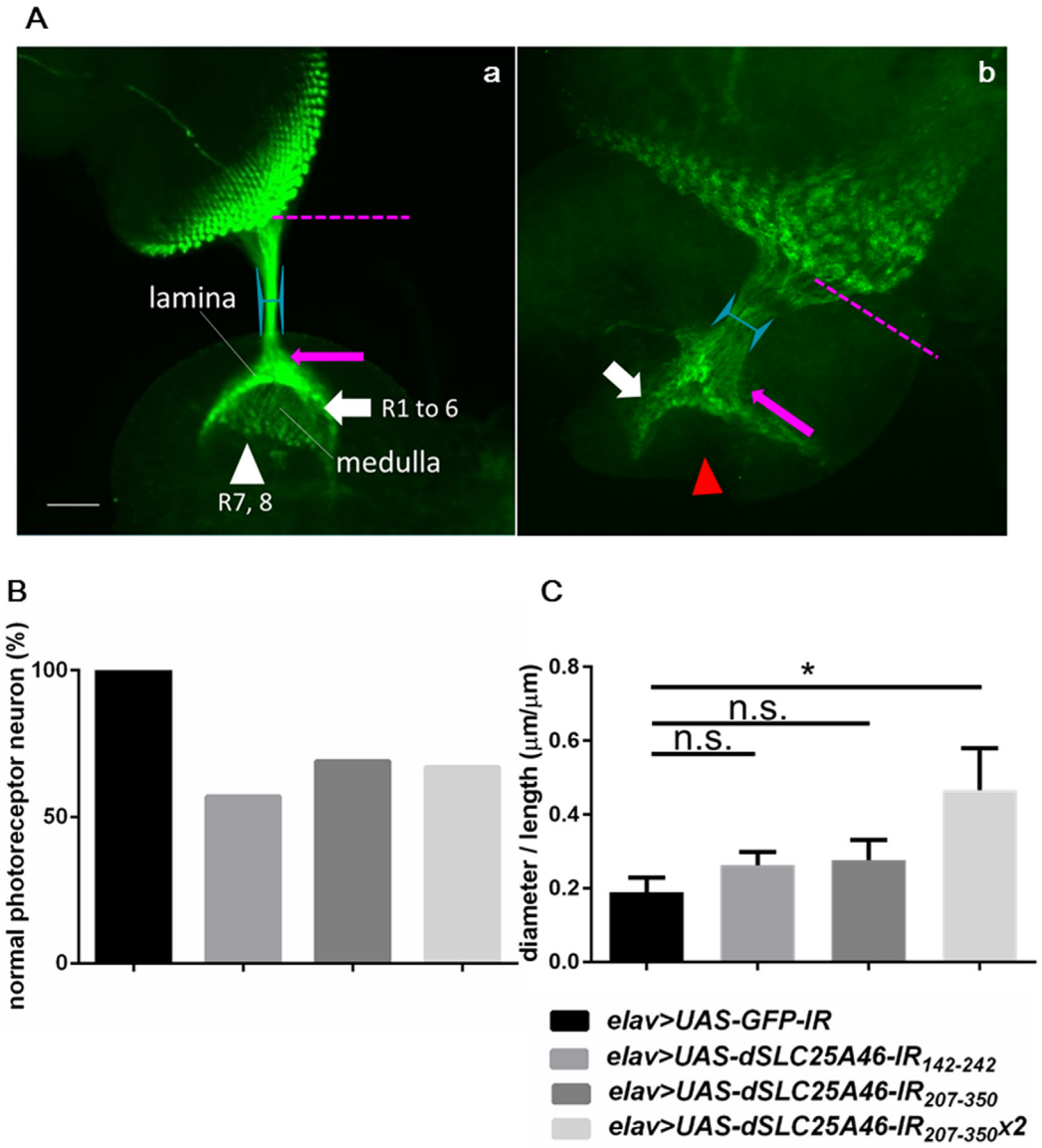

Fig. 10. Knockdown of *dSLC25A46* induces axonal targeting aberrations and abnormal morphology of photoreceptor neuron. (A) Immunostaining of photoreceptor neurons with anti-Chaoptin IgG. White arrow indicates the medulla region where R1–R6 innervate, and white arrowhead indicates the medulla region where R7 and R8 extend (a). Red arrowheads indicate aberrations of R7 and R8 axon targeting in medulla (b). Measured diameters of optic stalk are indicated by blue. Measured length of optic stalk (from dotted line to arrow) are indicated by magenta. The bars indicate 50 μm. (B, C) The quantified data. (B) In *dSLC25A46* knockdown larvae, R1–R6 photoreceptor cell neurons project to lamina normally, while aberrations in projection of R7–R8 into medulla were observed. (C) In *dSLC25A46* knockdown larvae, ratio of diameter per length are increased. *elav-GAL4 > UAS-GFP-IR* (*w; UAS-GFP-IR/+; elav-GAL4/+*), *elav-GAL4 > UAS-dSLC25A46-IR$_{142-242}$* (*w, UAS-dSLC25A46-IR$_{142-242}$/w; +; elav-GAL4/+*), *elav-GAL4 > UAS-dSLC25A46-IR$_{207-350}$* (*w; UAS-dSLC25A46-IR$_{207-350}$/+; elav-GAL4/+*), and *elav-GAL4 > UAS-dSLC25A46-IR$_{207-350}$x2* (*w; UAS-dSLC25A46-IR$_{207-350}$; elav-GAL4/+*).

effect. Accumulation of defective mitochondria likely occurs by lack of mitochondrial dynamics. This would then cause not only aberrant neuronal morphology but also reduction of active zone, an indicator of neuronal dysfunction in NMJs that finally results in defects in locomotive ability. In contrast, knockdown of *Marf* which is a *Drosophila* homolog of *MFN2*, another CMT causing gene, induces mitochondrial fragmentation with neuronal defect (Altanbyek et al., 2016; Sandoval et al., 2014). Therefore, proper regulation of mitochondrial dynamics appears to be important for proper neuronal function. Previous studies established other animal models targeting of *SLC25A46*. In zebrafish knockdown model, axon tracts in motoneurons were shortened. Mitochondria in motoneurons are not located in proper area and also appear to be aggregated, but they display normal swimming ability (Abrams et al., 2015). Mouse *SLC25A46* knockout model displayed impaired motility, frequently fused and aggregated mitochondria in Purkinje cells and optic atrophy (Li et al., 2017). Phenotypes induced by decreased level of *SLC25A46* are slightly different among different animal models. Functional analyses with various model organisms might be necessary to reveal the pathogenesis of human diseases caused by *SLC25A46*.

To eliminate the possible off-target effects of the used RNAi constructs, we examined two different *dSLC25A46* inverted repeat constructs (*UAS-dSLC25A46-IR$_{142-242}$* and *UAS-dSLC25A46-IR$_{207-350}$*). Target sequences for these two RNAi lines were designed to have no off-target effects (VDRC and online dsCheck software http://dscheck.rnai.jp). When these transgenic fly lines were crossed with the elav-GAL4 line to specifically express *dSLC25A46* dsRNA in neuronal tissues, each of independent fly strains showed essentially the same phenotype. These results thus demonstrate

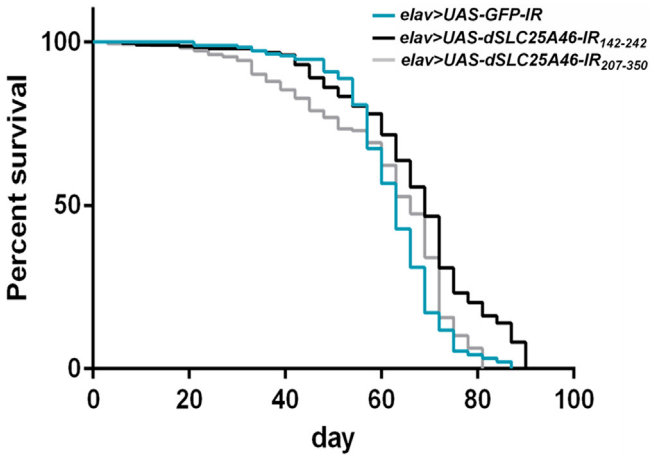

Fig. 11. Viability assay. The percentage of surviving flies carrying *elav-GAL4 > UAS-GFP-IR* (*w; UAS-GFP-IR/+; elav-GAL4/+*), *elav-GAL4 > UAS-dSLC25A46-IR$_{142-242}$* (*w, UAS-dSLC25A46-IR$_{142-242}$/w; +; elav-GAL4/+*), and *elav-GAL4 > UAS-dSLC25A46-IR$_{207-350}$* (*w; UAS-dSLC25A46-IR$_{207-350}$/+; elav-GAL4/+*) is shown. *dSLC25A46* knockdown does not affect in the lifespan of adult flies. (Log-rank test, n = 100).

that the phenotypes observed with the neuron-specific *dSLC25A46*-knockdown flies are not due to an off-target effect but rather to a reduction in dSLC25A46 protein levels.

It is known that *SLC25A46* mutations in human cause optic atrophy. According to previous studies, optic stalk morphology and development in *Drosophila* are precisely regulated via cell proliferation and migration. Previous study identified the *Focal adhesion kinase56D* (*Fak56D*) gene as an important component required for optic stalk formation (Murakami et al., 2007). *Fak56D* is a *Drosophila* homolog of mammalian focal adhesion kinase (FAK; also known as Ptk2), that is a main regulatory component of focal contacts (Mitra et al., 2005; Parsons, 2003). Mutation in *Fak56D* causes random distribution of cells that could not be arranged into a tubular structure and lose tendency to migrate along optic stalk. This could lead to broadened and shortened optic stalk (Murakami et al., 2007). In this study, immunocytochemical analyses of subcellular localization of dSLC25A46 revealed that dSLC25A46 localizes not only in mitochondria, but also in plasma membrane. These observations suggest that in addition to the role in mitochondrial function, plasma membrane-localized dSLC25A46 plays a role in cell proliferation and/or migration to control optic stalk formation. Although human SLC25A46 is reported to be mainly localized in mitochondria (Abrams et al., 2015), these studies have been limited to cultured cells. The present in vivo study in *Drosophila* suggests the possibility that human SLC25A46 may be localized not only in mitochondria but also in plasma membranes in human optic axons.

In conclusion, our *dSLC25A46* knock-down *Drosophila* model recapitulates most of the phenotypes in mitochondrial disease patients, providing a useful tool to study these diseases. Considering the successful use of *Drosophila* model to identify genetic interactants with the causing genes for various neurodegenerative diseases (Azuma et al., 2014; Shimamura et al., 2014), extensive genetic screen with the neuron-specific *dSLC25A46*-knockdown flies will allow us to identify genes and signaling pathways that are related to *dSLC25A46* function in neuron. These genes and pathways could be promising targets for therapy of mitochondrial diseases including CMT. Therefore, the neuron-specific *dSLC25A46*-knockdown flies established in this study could be a useful model to search novel therapeutic target of both of these syndromes and candidate substances for therapy. Moreover, given the similar phenotypes between CMT fly models established by knockdown (Kyotani et al., 2016) or deletion (Bharadwaj et al., 2016, p. 4) of *dfig4* and knockdown of *dSLC25A46*, these genes could involve in common pathological mechanisms of neurodegeneration, which opens the possibility of future pathway-oriented therapy for CMT.

4. Experimental procedure

4.1. Fly stocks

Flies were reared on standard food containing 0.65% agar, 10% glucose, 4% dry yeast, 5% cone flour, and 3% rice bran at 25 °C. Canton S was used as the wild type. *w UAS-dSLC25A46-IR$_{142-242}$; +; +* and *w; UAS-dSLC25A46-IR$_{207-350}$; +* (CG5755) were obtained from the Vienna *Drosophila* Resource Center (VDRC). The RNAi of these strain was targeted to the region corresponding to amino acid residues (aa) *142–242* or *207–350* of *Drosophila* SLC25A46. The fly line carrying *w; P{UAS-GFP.dsRNA.R}143, w*; *P[GAL4-elav.L]^{3}* was obtained from the Bloomington *Drosophila* Stock Center (BDSC) at Indiana University. In addition, *w; UAS-beta-gal-IR; +* (VDRC) and *w; P[GawB]D42 P[w^{+mC} = UAS-mitoGFP.AP]3/P[GawB]D42 P[w^{+mC} = UAS-mitoGFP.AP]3* (BDSC) were also used to study the mitochondrial localization in neuromuscular junctions.

4.2. Comparison of amino acid sequences of human SLC25A46, and Drosophila SLC25A46

The amino acid (aa) sequence of *Drosophila* SLC25A46 was retrieved from UniProt (http://www.uniprot.org). The identity and similarity of human SLC25A46 and *Drosophila* SLC25A46 were compared using FASTA and BLAST.

4.3. Production of rabbit anti-dSLC25A46 antibody

The dSLC25A46 peptide Cys-NKSSTTKSPSISSI-OH, corresponding to aa423-436 of dSLC25A46 was conjugated to keyhole limpet hemocyanin and mixed with Freund's complete adjuvant to provide a suspension. The underlined N-terminal residue Cys was an added residue. Then the suspension was injected subcutaneously into a rabbit (Japanese White) kept under specific pathogen-free conditions. The rabbit was then boosted with inoculations of an immunogen of the same quality once a week for 7 weeks, and a terminal bleed was performed to collect the maximum amount of serum (Scrum Inc.).

4.4. Flip out experiments

RNAi clones in *Drosophila* larval salivary gland were generated with a flip-out system (Sun and Tower, 1999). Female flies with *hs-flp; Act5C > FRT y FRT > GAL4, UAS-GFP* were crossed with male flies carrying *UAS-dSLC25A46-IR$_{207-350}$*. Clones were evaluated by the presence of green fluorescent protein (GFP) expressed under control of the *Act5C* promoter. Flip-out was induced by heat shock (60 min at 37 °C) at 24–48 h after egg laying.

4.5. Immunostaining with anti-dSLC25A46 antibody

For immunohistochemistry, larval salivary glands were dissected, and fixed in 4% paraformaldehyde/PBS for 20 min at 25 °C. After washing with PBS containing 0.3% Triton X-100, the samples were blocked with PBS containing 0.15% Triton X-100 and 10% normal goat serum for 30 min at 25 °C. Then the samples were incubated with diluted primary antibodies in PBS containing 0.15% Triton X-100 and 10% normal goat serum for 16 h at 4 °C. The following antibodies were used as primary antibodies: rabbit anti- dSLC25A46 antibody (1:50), mouse anti-Dlg (1:400) (Developmental Studies of Hybridoma Bank, DSHB), mouse anti-KDEL

(1:800) (Enzo Life Sciences), mouse anti-KDEL receptor (1:300) (Abcam), mouse anti-HSP60 (1:200) (Enzo Life Sciences). After washing with PBS containing 0.3% Triton X-100, samples were incubated with secondary antibodies labeled with Alexa 594 (1:400) and 488 (1:400) for 3 h at 25 °C. After washing with PBS containing 0.3% Triton X-100, the samples were stained with DAPI (0.5 μg/ml)/PBS/0.1% Triton X-100. After washing with PBST and PBS, samples were then mounted in the Vectashield (Vector laboratories) and inspected by a confocal laser scanning microscopy (Olympus Fluoview FV10i).

4.6. Western blot analysis

Protein extracts from the CNS of twenty larvae carrying *w*; *UAS-GFP-IR*/+; *elav-GAL4*/+, *w*, *UAS-dSLC25A46-IR*$_{142–242}$/*w*; +; *elav-GAL4*/+, *w*; *UAS-dSLC25A46-IR*$_{207–350}$/+; *elav-GAL4*/+, *w*; *UAS-dSLC25A46-IR*$_{207–350}$; *elav-GAL4*/+ were prepared. In brief, twenty larval CNS were boiled at 95 °C for 2 min in 0.1 M Tris-HCl (pH 7.6) and complete Mini, EDTA-free (Roche Diagnostics) and homogenized in sample buffer containing 50 mM Tris-HCl (pH 6.8), 2% sodium dodecyl sulfate (SDS), 10% glycerol, 0.1% bromophenol blue and 1.2% β-mercaptoethanol. The homogenates were then boiled at 95 °C for 5 min followed by centrifugation. The supernatants containing protein extracts were electrophoretically separated on SDS-polyacrylamide gels containing 6% acrylamide and then transferred to polyvinylidene difluoride membranes (Bio-Rad). The blotted membranes were preincubated with TBS/0.1% Tween 20 containing 0.3% skim milk for 1 h at 25 °C and incubated with rabbit anti-dSLC25A46 antibody (1:500) for 16 h at 4 °C. After repeated washing, the membrane was incubated with horseradish peroxidase (HRP)-conjugated anti-rabbit IgG (1:4000) in for 1 h at 25 °C. Antibody binding was detected using ECL-advance Western blotting detection reagents, and images were analyzed with ImageJ (NIH, USA). To ensure equal protein loading in each lane, the membranes were also probed with a rabbit anti-α-tubulin antibody at the same time and HRP-conjugated anti-rabbit IgG. For detection of α-tubulin in some cases, mouse anti-α-tubulin monoclonal antibody (1:8000, Sigma) and HRP-conjugated anti-mouse IgG (1:10,000, GE Healthcare) were also used as the primary and secondary antibodies, respectively.

4.7. RNA isolation and quantitative RT-PCR (qRT-PCR)

Ten larval CNS were dissected and kept in liquid nitrogen. Then, total RNA was isolated using a RNeasy Lipid Tissue Mini Kit (Qiagen). The synthesis of cDNA was then performed using a PrimeScript™ RT Reagent Kit (Takara). Finally, a Bio-Rad CFX96TM Real-Time System was used in order to perform qRT-PCR with SYBR® Premix Ex Taq™ (Tli RNase H Plus) (Takara) and target-specific primers. The data were analyzed by a standard curve-based method calculated using CFX ManagerTM software. Specificity of primers was tested using melting curves created with CFX ManagerTM software. GAPDH mRNA was used as an internal control. *Drosophila* whole genomic nucleotide sequences used for primer design were based on the FlyBase online database. Primer sequences are listed below.*dSLC25A46* forward primer: 5′-TCGAATGATGCAGAGGAGAATG-3′*dSLC25A46* reverse primer: 5′-CTCAGTGGTAAGCATGGCTATAA-3′

GAPDH forward primer: 5′-GGAGCCACCTATGACGAAATC-3′

GAPDH reverse primer: 5′-TCGAACACAGACGAATGGG-3′

4.8. Crawling assay

The crawling assay was performed as described previously (Nichols et al., 2012) with some modifications. Female larvae in the early third instar stage were collected and washed with PBS to remove food traces. Then larvae were transferred to agar plates containing 2% agar at a density of two or three larvae per plate. Larval movement was recorded using a digital camera for 1 min. The recorded videos were converted into AVI type using a MOV to AVI converter (Pazera Jacek, Poland) and then analyzed using ImageJ (NIH, USA) with a wrMTrck plugin (developed by Dr. Jesper Søndergaard Pedersen) to track larval movement and draw motion paths.

4.9. Climbing assay

The climbing assay was performed as described previously with minor modifications (Kyotani et al., 2016). Newly eclosed adult female flies were collected and separated into vials at a maximum density of 20 flies per vial. Flies were then transferred to a conical tube without anesthesia. After that, the tubes were tapped to collect the flies to the bottom, and the length of time required for adult flies to climb was recorded for 5 s. These procedures were repeated five times and recorded using a digital camera. For all of the climbing experiments, the height to which each fly climbed was scored as follows; 0 (<2 cm), 1 (between 2 and 4 cm), 2 (between 4 and 6 cm), 3 (between 6 and 8 cm), 4 (between 8 and 10 cm), and 5 (more than 10 cm). The climbing assays were performed every seven days from day 1 after enclosion.

4.10. Visualization of neuromuscular junctions

For the visualization of NMJs, third instar larvae were dissected in HL3 saline and fixed with 4% paraformaldehyde in PBS for 30 min at 25 °C. After being washed, the samples were blocked with PBS containing 0.15% Triton X-100 and 10% NGS for 30 min at 25 °C and incubated with primary antibodies in PBS containing 0.15% Triton X-100 and 10% NGS for 16 h at 4 °C. The following antibodies were used; rabbit anti-GFP IgG (1:200, Medical & Biological Laboratories [MBL], 598), mouse anti-Dlg (1:500, DSHB, 4F3), mouse anti-Brp IgG (1:200, DSHB, nc82). After being washed with PBS containing 0.3% Triton X-100, samples were incubated with secondary antibodies labeled with Alexa 594 (1:400) and 488 (1:400) or, 594 (1:400) and FITC-conjugated goat anti-HRP IgG (1:400) for 3 h at 25 °C. After extensive washing with PBS containing 0.3% Triton X-100, samples were mounted with Vectashield (Vector Laboratories) for laser confocal microscope or ProLong Diamond (Invitrogen) for super resolution microscope. Confocal microscopic images were taken with a confocal laser scanning microscope (Olympus Fluoview FV10i) and processed with MetaMorph software (Molecular devices). Images of samples were also taken with a super resolution microscope (N-SIM, Nikon)

4.11. Visualization of photoreceptor neuron

For immunohistochemistry, larval eye imaginal discs were dissected, and fixed in 4% paraformaldehyde/PBS for 15 min at 25 °C. After washing with PBS containing 0.3% Triton X-100, the samples were blocked with PBS containing 0.15% Triton X-100 and 10% normal goat serum for 30 min at 25 °C, and incubated with diluted primary antibodies in PBS containing 0.15% Triton X-100 and 10% normal goat serum for 16 h at 4 °C. mouse anti-Chaoptin (1:100, DSHB 24B10) antibody was used. After washing with PBS containing 0.3% Triton X-100, samples were incubated with secondary antibodies labeled with either Alexa 488 or Alexa 594 (1:400, Invitrogen) for 3 h at 25 °C. After extensive washing with PBS containing 0.3% Triton X-100, samples were mounted in the Vectashield (Vector laboratories) and analyzed by a confocal laser scanning microscopy (Olympus Fluoview FV10i).

4.12. ROS detection

Levels of ROS were detected by CM-H_2DCFDA (Thermo Fisher Scientific). In 1% CM-H_2DCFDA /PBS, larval CNS were shaken 15sec. After 10 min incubation and extensive washing with PBS, samples were mounted in the Vectashield (Vector laboratories) and inspected by a confocal laser scanning microscopy (Olympus Fluoview FV10i).

4.13. ATP measurement

CellTiter-Glo (Promega) were used for measuring ATP level. After homogenizing ten larval CNS in 100μL of ATP assay buffer (Abcam), samples centrifuged (4°C, 5 min at 13,000×*g*). The supernatant was then removed into the microtubule, 10μL of cold trichloroacetic acid (Abcam) and keep the sample on ice for 15 min. After centrifugation at 12,000×*g* for 5 min, 10 μL neutralization solution (ab204708, Abcam) was added and allowed to rest for 5 min on ice. 50 μL samples and 50 μL Celltiter-Glo were mixed to each well. Luminescence was read on Lumat LB 9507 (Berthold Technologies).

4.14. Lifespan assay

The parent flies were placed at 28 °C, and newly eclosed adult female flies were separated into vials at a low density (20 flies per vial) and maintained in a humidified, temperature controlled incubator at 25 °C and 60% humidity in a 12 h light and 12 h dark cycle. The flies were then transferred to new tubes containing fresh food, and deaths were scored every three days. Survival rate was determined by the percentage of surviving flies from day to day until all flies died.

4.15. Immunizing peptide competition experiments

Immunostaining methods are essentially same as Section 4.5. The rabbit anti-dSLC25A46 antibody was pretreated with 20 μg of blocking dSLC25A46 peptide (Cys-NKSSTTKSPSISSI-OH). The samples were incubated with the pretreated rabbit anti-dSLC25A46 antibody (1:50 dilution) in PBS containing 0.15% Triton X-100 and 1% bovine serum albumin for 16 h at 4 °C.

4.16. Data analysis

GraphPad Prism 6 was used to analyze the statistics of all results except for the climbing assay. In the Western blot analysis, crawling assay, NMJ and photoreceptor neuron visualization, ROS detection, and ATP measurement, the P-values were calculated by using unpaired Welch's *t*-test (one-tailed). For the statistics of climbing assay, the SPSS software (IBM) was used. All data are shown as means ± SEM. Lifespan assay results were evaluated using a log-rank test.

Acknowledgements

We thank the Bloomington *Drosophila* Stock Center, Vienna *Drosophila* Genetic Resource Center, and Kyoto Stock Center for fly lines. This study was partially supported by the JSPS Core-to-Core Program, Asia-Africa Science Platforms, JSPS Program for Advancing Strategic International Networks to Accelerate the Circulation of Talented Researchers (Grant No. S2802). JSPS KAKENHI Grant Number 16K07346.

Competing financial interests

The authors declare no competing financial interests in relation to the work described.

Appendix A. Supplementary data

Supplementary data associated with this article can be found, in the online version, at https://doi.org/10.1016/j.brainres.2018.03.028.

References

Abrams, A.J., Hufnagel, R.B., Rebelo, A., Zanna, C., Patel, N., Gonzalez, M.A., Campeanu, I.J., Griffin, L.B., Groenewald, S., Strickland, A.V., Tao, F., Speziani, F., Abreu, L., Schüle, R., Caporali, L., La Morgia, C., Maresca, A., Liguori, R., Lodi, R., Ahmed, Z.M., Sund, K.L., Wang, X., Krueger, L.A., Peng, Y., Prada, C.E., Prows, C.A., Schorry, E.K., Antonellis, A., Zimmerman, H.H., Abdul-Rahman, O.A., Yang, Y., Downes, S.M., Prince, J., Fontanesi, F., Barrientos, A., Németh, A.H., Carelli, V., Huang, T., Zuchner, S., Dallman, J.E., 2015. Mutations in SLC25A46, encoding a UGO1-like protein, cause an optic atrophy spectrum disorder. Nat. Genet. 47, 926–932. https://doi.org/10.1038/ng.3354.

Altanbyek, V., Cha, S.-J., Kang, G.-U., Im, D.S., Lee, S., Kim, H.-J., Kim, K., 2016. Imbalance of mitochondrial dynamics in Drosophila models of amyotrophic lateral sclerosis. Biochem. Biophys. Res. Commun. 481, 259–264. https://doi.org/10.1016/j.bbrc.2016.10.134.

Azuma, Y., Tokuda, T., Shimamura, M., Kyotani, A., Sasayama, H., Yoshida, T., Mizuta, I., Mizuno, T., Nakagawa, M., Fujikake, N., Ueyama, M., Nagai, Y., Yamaguchi, M., 2014. Identification of *ter94*, *Drosophila VCP*, as a strong modulator of motor neuron degeneration induced by knockdown of *Caz*, *Drosophila FUS*. Hum. Mol. Genet. 23, 3467–3480.

Bharadwaj, R., Cunningham, K.M., Zhang, K., Lloyd, T.E., 2016. FIG4 regulates lysosome membrane homeostasis independent of phosphatase function. Hum. Mol. Genet. 25, 681–692. https://doi.org/10.1093/hmg/ddv505.

Charlesworth, G., Balint, B., Mencacci, N.E., Carr, L., Wood, N.W., Bhatia, K.P., 2016. SLC25A46 mutations underlie progressive myoclonic ataxia with optic atrophy and neuropathy. Mov. Disord. 31, 1249–1251. https://doi.org/10.1002/mds.26716.

Charroux, B., Royet, J., 2013. Mutations in the Drosophila ortholog of the vertebrate Golgi pH regulator (GPHR) protein disturb endoplasmic reticulum and Golgi organization and affect systemic growth. Biol. Open 3, 72–80. https://doi.org/10.1242/bio.20137187.

Chow, C.Y., Reiter, L.T., 2017. Etiology of human genetic disease on the fly. Trends Genet. TIG 33, 391–398. https://doi.org/10.1016/j.tig.2017.03.007.

Haitina, T., Lindblom, J., Renström, T., Fredriksson, R., 2006. Fourteen novel human members of mitochondrial solute carrier family 25 (SLC25) widely expressed in the central nervous system. Genomics 88, 779–790. https://doi.org/10.1016/j.ygeno.2006.06.016.

Hediger, M.A., Romero, M.F., Peng, J.-B., Rolfs, A., Takanaga, H., Bruford, E.A., 2004. The ABCs of solute carriers: physiological, pathological and therapeutic implications of human membrane transport proteins. Pflüg. Arch. 447, 465–468. https://doi.org/10.1007/s00424-003-1192-y.

Huu, N.T., Yoshida, H., Umegawachi, T., Miyata, S., Yamaguchi, M., 2014. Structural characterization and subcellular localization of Drosophila organic solute carrier partner 1. BMC Biochem. 15, 11. https://doi.org/10.1186/1471-2091-15-11.

Janer, A., Prudent, J., Paupe, V., Fahiminiya, S., Majewski, J., Sgarioto, N., Des Rosiers, C., Forest, A., Lin, Z.-Y., Gingras, A.-C., Mitchell, G., McBride, H.M., Shoubridge, E. A., 2016. SLC25A46 is required for mitochondrial lipid homeostasis and cristae maintenance and is responsible for Leigh syndrome. EMBO Mol. Med. 8, 1019–1038 https://doi.org/10.15252/emmm.201506159.

Keshishian, H., Broadie, K., Chiba, A., Bate, M., 1996. The drosophila neuromuscular junction: a model system for studying synaptic development and function. Annu. Rev. Neurosci. 19, 545–575. https://doi.org/10.1146/annurev.ne.19.030196.002553.

Kyotani, A., Azuma, Y., Yamamoto, I., Yoshida, H., Mizuta, I., Mizuno, T., Nakagawa, M., Tokuda, T., Yamaguchi, M., 2016. Knockdown of the *Drosophila FIG4* induces deficient locomotive behavior, shortening of motor neuron, axonal targeting aberration, reduction of life span and defects in eye development. Exp. Neurol. 277, 86–95. https://doi.org/10.1016/j.expneurol.2015.12.011.

Lewis, M.J., Pelham, H.R., 1992. Sequence of a second human KDEL receptor. J. Mol. Biol. 226, 913–916.

Lewis, M.J., Pelham, H.R., 1990. A human homologue of the yeast HDEL receptor. Nature 348, 162–163. https://doi.org/10.1038/348162a0.

Li, Z., Peng, Y., Hufnagel, R.B., Hu, Y.-C., Zhao, C., Queme, L.F., Khuchua, Z., Driver, A. M., Dong, F., Lu, Q.R., Lindquist, D.M., Jankowski, M.P., Stottmann, R.W., Kao, W. W.Y., Huang, T., 2017. Loss of SLC25A46 causes neurodegeneration by affecting mitochondrial dynamics and energy production in mice. Hum. Mol. Genet. 26, 3776–3791. https://doi.org/10.1093/hmg/ddx262.

Mitra, S.K., Hanson, D.A., Schlaepfer, D.D., 2005. Focal adhesion kinase: in command and control of cell motility. Nat. Rev. Mol. Cell Biol. 6, 56–68. https://doi.org/10.1038/nrm1549.

Munro, S., Pelham, H.R., 1987. A C-terminal signal prevents secretion of luminal ER proteins. Cell 48, 899–907.
Murakami, S., Umetsu, D., Maeyama, Y., Sato, M., Yoshida, S., Tabata, T., 2007. Focal adhesion kinase controls morphogenesis of the Drosophila optic stalk. Development 134, 1539–1548. https://doi.org/10.1242/dev.001529.
Nguyen, M., Boesten, I., Hellebrekers, D.M.E.I., Mulder-den Hartog, N.M., de Coo, I.F. M., Smeets, H.J.M., Gerards, M., 2017. Novel pathogenic SLC25A46 splice-site mutation causes an optic atrophy spectrum disorder. Clin. Genet. 91, 121–125. https://doi.org/10.1111/cge.12774.
Nichols, C.D., Becnel, J., Pandey, U.B., 2012. Methods to assay Drosophila behavior. J. Vis. Exp. https://doi.org/10.3791/3795.
Niehues, S., Bussmann, J., Steffes, G., Erdmann, I., Köhrer, C., Sun, L., Wagner, M., Schäfer, K., Wang, G., Koerdt, S.N., Stum, M., Jaiswal, S., RajBhandary, U.L., Thomas, U., Aberle, H., Burgess, R.W., Yang, X.-L., Dieterich, D., Storkebaum, E., 2016. Corrigendum: impaired protein translation in Drosophila models for charcot-marie-tooth neuropathy caused by mutant tRNA synthetases. Nat. Commun. 7, 10497. https://doi.org/10.1038/ncomms10497.
Palmieri, F., 2013. The mitochondrial transporter family SLC25: identification, properties and physiopathology. Mol. Aspects Med. 34, 465–484. https://doi.org/10.1016/j.mam.2012.05.005.
Parsons, J.T., 2003. Focal adhesion kinase: the first ten years. J. Cell Sci. 116, 1409–1416.
Pelham, H.R., 1990. The retention signal for soluble proteins of the endoplasmic reticulum. Trends Biochem. Sci. 15, 483–486.
Pelham, H.R., 1988. Evidence that luminal ER proteins are sorted from secreted proteins in a post-ER compartment. EMBO J. 7, 913–918.
Pilling, A.D., Horiuchi, D., Lively, C.M., Saxton, W.M., 2006. Kinesin-1 and Dynein are the primary motors for fast transport of mitochondria in Drosophila motor axons. Mol. Biol. Cell 17, 2057–2068. https://doi.org/10.1091/mbc.E05-06-0526.
Rask-Andersen, M., Masuram, S., Fredriksson, R., Schiöth, H.B., 2013. Solute carriers as drug targets: Current use, clinical trials and prospective. Mol. Aspects Med. 34, 702–710. https://doi.org/10.1016/j.mam.2012.07.015. The ABCs of membrane transporters in health and disease (SLC series).
Sandoval, H., Yao, C.-K., Chen, K., Jaiswal, M., Donti, T., Lin, Y.Q., Bayat, V., Xiong, B., Zhang, K., David, G., Charng, W.-L., Yamamoto, S., Duraine, L., Graham, B.H., Bellen, 2014. Mitochondrial fusion but not fission regulates larval growth and synaptic development through steroid hormone production. eLife 3. https://doi.org/10.7554/eLife.03558.
Shimamura, M., Kyotani, A., Azuma, Y., Yoshida, H., Nguyen, T.B., Mizuta, I., Yoshida, T., Mizuno, T., Nakagawa, M., Tokuda, T., Yamaguchi, M., 2014. Genetic link between *Cabeza*, a *Drosophila* homologue of *Fused in Sarcoma* (*FUS*), and the EGFR signaling pathway. Exp. Cell. Res. 326, 36–45.
Soltys, B.J., Gupta, R.S., 1996. Immunoelectron microscopic localization of the 60-kDa heat shock chaperonin protein (Hsp60) in mammalian cells. Exp. Cell Res. 222, 16–27. https://doi.org/10.1006/excr.1996.0003.
Steffen, J., Vashisht, A.A., Wan, J., Jen, J.C., Claypool, S.M., Wohlschlegel, J.A., Koehler, C.M., 2017. Rapid degradation of mutant SLC25A46 by the ubiquitin-proteasome system results in MFN1/2-mediated hyperfusion of mitochondria. Mol. Biol. Cell 28, 600–612. https://doi.org/10.1091/mbc.E16-07-0545.
Storkebaum, E., Leitão-Gonçalves, R., Godenschwege, T., Nangle, L., Mejia, M., Bosmans, I., Ooms, T., Jacobs, A., Van Dijck, P., Yang, X.-L., Schimmel, P., Norga, K., Timmerman, V., Callaerts, P., Jordanova, A., 2009. Dominant mutations in the tyrosyl-tRNA synthetase gene recapitulate in Drosophila features of human Charcot-Marie-Tooth neuropathy. Proc. Natl. Acad. Sci. U.S.A. 106, 11782–11787. https://doi.org/10.1073/pnas.0905339106.
Sun, J., Tower, J., 1999. FLP recombinase-mediated induction of Cu/Zn-superoxide dismutase transgene expression can extend the life span of adult drosophila melanogaster flies. Mol. Cell. Biol. 19, 216–228.
Tang, B.L., Wong, S.H., Qi, X.L., Low, S.H., Hong, W., 1993. Molecular cloning, characterization, subcellular localization and dynamics of p23, the mammalian KDEL receptor. J. Cell Biol. 120, 325–338.
Teasdale, R.D., Jackson, M.R., 1996. Signal-mediated sorting of membrane proteins between the endoplasmic reticulum and the golgi apparatus. Annu. Rev. Cell Dev. Biol. 12, 27–54. https://doi.org/10.1146/annurev.cellbio.12.1.27.
Wan, J., Steffen, J., Yourshaw, M., Mamsa, H., Andersen, E., Rudnik-Schöneborn, S., Pope, K., Howell, K.B., McLean, C.A., Kornberg, A.J., Joseph, J., Lockhart, P.J., Zerres, K., Ryan, M.M., Nelson, S.F., Koehler, C.M., Jen, J.C., 2016. Loss of function of SLC25A46 causes lethal congenital pontocerebellar hypoplasia. Brain 139, 2877–2890. https://doi.org/10.1093/brain/aww212.